



HAL
open science

A dissipative model for deep-drawing simulations: Elastic springback prediction and incremental forming strategies

Y. Denis, N. Hamila, M. Itskov, E. Guzman-Maldonado, Fabrice Morestin

► To cite this version:

Y. Denis, N. Hamila, M. Itskov, E. Guzman-Maldonado, Fabrice Morestin. A dissipative model for deep-drawing simulations: Elastic springback prediction and incremental forming strategies. Composites Part A: Applied Science and Manufacturing, 2021, 149, 10.1016/j.compositesa.2021.106547 . hal-03660007

HAL Id: hal-03660007

<https://hal.science/hal-03660007>

Submitted on 2 Aug 2023

HAL is a multi-disciplinary open access archive for the deposit and dissemination of scientific research documents, whether they are published or not. The documents may come from teaching and research institutions in France or abroad, or from public or private research centers.

L'archive ouverte pluridisciplinaire **HAL**, est destinée au dépôt et à la diffusion de documents scientifiques de niveau recherche, publiés ou non, émanant des établissements d'enseignement et de recherche français ou étrangers, des laboratoires publics ou privés.



Distributed under a Creative Commons Attribution - NonCommercial 4.0 International License

A dissipative model for deep-drawing simulations: elastic springback prediction and incremental forming strategies

Y. Denis^a, N. Hamila^{b,*}, M. Itskov^c, E. Guzman-Maldonado^d, F. Morestin^e

^a*IRT Jules Verne, Chemin du Chaffault, 44340 Bouguenais, France*

^b*Ecole Nationale d'Ingénieurs de Brest, ENIB, UMR CNRS 6027, IRDL, F-29200, Brest, France*

^c*Department of Continuum Mechanics, RWTH Aachen University, Templergraben 55, 52056 Aachen, Germany*

^d*Innovamics, 87 Avenue des frères Perret, F69190 Saint Fons, France*

^e*Université de Lyon, INSA-Lyon, LaMCoS UMR 5259, Avenue Jean Capelle O, F69621 Villeurbanne Cedex, France*

Abstract

In industrial applications, with geometries of fabric and textile composites becoming more and more complex, new deep drawing strategies are required. In this context, modern incremental forming strategies appear to be very advantageous. Moreover, recent approaches have emerged making it possible to reach decent conclusions about the incremental forming strategy and the ability to predict the elastic spring back as well as the residual stresses in a draped woven fabric. The aims of this paper were thus several. The first part presents a discussion of the differences between classical models (often hyperelastic) and new ones (dissipative, hysteretical) under large strains. Subsequently, these models were compared in application to different deep-drawing geometries. It was found that more sophisticated models were interesting for complex forming, while common hyperelastic ones were efficient enough for simple geometries. The last part introduces some results concerning spring-back and new capabilities obtained by such dissipative models. Finally, two incremental forming tool geometries were also presented and discussed.

Keywords: Fabrics/textiles, Incremental Forming, Spring-back, Composite reinforcement, Large strains

1. Introduction

The field of composite materials opens up possibilities for a very wide range of applications. The use of such materials is becoming more and more common in aeronautics, automobiles or even medicine. This growth can be explained in particular by the favorable weight/characteristics ratio that composites offer. Indeed, mechanical characteristics in tension/compression, out-of-plane bending [1–4] and in-plane shear [5–8] are rather advantageous relative to the density of these materials.

Composites are often made up of various elements giving their individual geometrical and mechanical characteristics (type of weaving, fiber density, etc.) to the whole. These characteristics are important because

*Corresponding author

Email address: nahiene.hamila@enib.fr (N. Hamila)

they have a significant and direct impact on the shaping capacities, on the formation of wrinkles and, ultimately, on the structural health of the final part. Thus, depending on the type of composite, the forming processes can range from simple and controlled methods to much more delicate processes which are still the subject of intensive research and discussion.

A composite is often made up of a reinforcement and a matrix. The reinforcement gives most of the mechanical characteristics, whereas the matrix, often a resin, allows for good cohesion and maintains the deformed shape of the composite reinforcement. The work presented in this article focuses solely on the shaping of the dry reinforcement, and does not take into account the resin which is the case when using the Resin Transfer Molding (RTM) forming process [9, 10]. This process is divided into three stages, where the first is a phase of geometrical transformation of the woven fabric by the use of a punch/die pair. Secondly, the resin in its molten state is injected; a step that can be carried out either in situ using the same die/punch pair or by employing another press set-up. In the second case, the reinforcement must be moved from one set-up to another. This is the case, for example, for BMW parts [11]. Finally, once the resin has been injected and crystallized, the part can be removed from the mold.

The complexity of this kind of process leads to very high set-up costs. Many parameters must be taken into account and it is difficult to anticipate the right deep-drawing strategy. Thus, the use of a digital tool capable of predicting the orientation as well as stresses undergone by the material, or potential defects or damaged zones is strongly advised.

However, mechanical models and constitutive laws are not necessarily adapted to such processes. Indeed, most of the mechanical models used in forming simulations are based on non-linear elasticity [12–22]. Often more simple, easily adaptable and identifiable, they nevertheless have certain limits. For example, if the process requires the transfer of the dry reinforcement between the deformation phase and the injection phase, these latter models do not predict the elastic spring-back of the woven fabric. However, in case of complex process or complex forming, this lack of information leads to geometrical distortions or residual stresses not being properly considered. Indeed, an elastic or hyperelastic model does not describe the dissipated energy (which is mainly caused by friction between the warp and weft [23, 24]) or plastic deformations. [Since the spring-back is related to the release of the stored energy, if the dissipation is not considered while unloading, all energy generated by the deformation will be restored. Moreover, it is shown in this work that dissipative modelling is irrelevant for simple geometries conducting to monotonic loadings.](#) On the contrary, for other processes such as thermoforming, plenty of non-linear approaches [25–27] can take into account this dissipative behavior for example within the framework of viscoelasticity.

The objective of the present paper was, first to give a quick presentation of a new elastoplasticity model [28, 29] taking into account the hysteretic behavior of the material. Such a model has recently been developed [30–36] and enables to push the limits of hyperelastic simulations. Previous experimental work has also shown that fabric materials exhibit dissipative/hysteretic behaviors [24, 37–39].

In addition, recent studies have led to propositions of new forming strategies in order to limit defects and optimize stress and strain distributions in the material. For example, the use of incremental shaping [40–43], requires several punches for a single mold. Often, the use of blank-holders may also apply cyclic loads to the reinforcement. Hyperelastic models do not take into account these variations of loads so that the simulation results of complex processes or geometries are not necessarily representative and reliable.

Finally, the hysteretic models used in this paper have focused only on the in-plane shear and the out-of-plane bending deformation modes. Indeed, fibers are considered quasi-inextensible and can thus be described by a hyperelastic model under tension.

Thus, the first part of this article presents a hysteretic approach and compares it with common hyperelastic ones. There are several methods that describe hysteresis, i.e. hysteretic behavior including an adaptation of the Mroz nested surfaces theory [44–48] or fractional derivatives [31, 33, 34]. In the second part, numerical examples with a simple hemisphere and more complex draping geometries are introduced. Finally, the incremental approaches are also discussed since this method opens up plenty of possibilities for the creation of composite fabrics in the case of a complex geometry. Finally, two examples are put forward on which the advantages and limitations of the proposed approach are discussed.

2. A hysteretic model: an innovative way to simulate composite forming

Usually, hyperelastic models used to simulate the forming of dry reinforcements in the RTM process. Due to their simplicity such models are relatively easy to identify and integrate into a finite element software. However, models of this kind cannot properly describe the mechanical behavior of the material. Indeed, in certain cases of draping of a complex shape, the simulation results do not coincide with experimental data (Fig. 9(b) and 9(d)). Thus, more sophisticated models, less trivial and more difficult to integrate into a finite element software, have recently been developed [17, 31, 32, 34]. These more complex models, make it possible to take into account strongly non-linear material behaviors. Moreover, a composite reinforcement will very often present a hysteretic behavior particularly difficult to describe. In [30–33], some first approaches and possibilities to describe such behaviors for dry fabrics are put forward.

The aim of the present section is not to go into detail of these approaches but rather to give an overview of these inelastic models and to outline the differences between hyperelastic and hysterical approaches. To this end, these approaches are compared from either a simulative or an experimental point of view. Simulation results are further compared to experimental data.

As mentioned in the introduction, the three main deformation modes when forming a composite reinforcement are the in-plane shear, the out-of-plane bending and the fiber tension. However, since [the deformation mechanism of a composite reinforcement assumes the inextensibility of the fibers, they are often described by elastic models, despite the fact that friction still occur at the microscopic scale.](#) Only the in-plane shear

and the out-of-plane bending are regarded as dissipative in the following.

2.1. Comparison between hyperelasticity and hystericity

The first part of this section focuses on the in-plane shear mode. The experimental behavior is determined from a picture frame test [49–51] with the woven fabric [Hexcel G1151](#)) presented in Table 1.

In Fig. 1 shear stresses are plotted versus shear strains resulting both from the experimental data, the hysteretic and the hyperelastic models. Fig. 1(a) shows the result of the hyperelastic behavior [19, 52] while Fig. 1(b) gives the outcome of the hysteretic model [31, 32]. Notations $P1$, $P2$, $P3$ and $P4$ in Fig. 1(b) and Fig. 2(b) refer to the different parts used to model each behavior. In Fig. 1(b), $P1$ and $P2$ refer to the upper/lower bounds for the dissipative path, $P3$ and $P4$ refer to the hysteresis loop (respectively for the decreasing and the growing part). In Fig. 2(b), $P1$ refers to the dissipative path while $P2$ and $P3$ describe the hysteresis loop.

As it can be seen, the experimental behavior of this fabric with a cyclical shear loading is highly non-linear and follows a hysteretic path described by hysteresis loops (four complete loops in this figure).

Finally, as displayed in Fig. 1(b), the hystericity is represented by a coupled method. The upper and lower bounds (phases $P1$, $P2$ and $P4$ are following a thermodynamically consistent theory and the phase $P3$ is purely mathematical and has not so far been proved to be thermodynamically consistent. However, with this approach, the number of required parameters remains low ([11 coefficients for 4 parameters needed](#)), and hence, programming the model in a finite element software becomes much easier. Complete details of such models for woven fabrics are presented in [31, 34] and in Appendix A.

The second main deformation mode is the out-of-plane bending shown in Fig. 2. Corresponding experimental data can be found in [1, 30, 31]. Even if the experimental data do not represent a cyclic bending load, the hysteresis loops are inspired by studies [1, 30] that describe the Kawabata bending test [53] commonly applied to metallic materials. [Since the fabric is balanced and regarding the literature \[1, 30, 54\], it is assumed that the bending behavior is the same in both warp or weft direction.](#) As before, Fig. 2(a) shows the application of a hyperelastic behavior whereas Fig. 2(b) displays predictions of the hysteretic model under cyclic loading.

The strategy used to model the bending behavior for deep-drawing simulations is based on the fractional derivatives theory.

Note that hystericity is of advantage in comparison to the hyperelastic model only under cyclical loading. More details about the influence of each model are given in section 2.3.

2.2. Application: set-up, material, lay-up and forming configurations

In this section the context for the study is discussed: the woven fabric, the model parameters, the three experimental sets-up for the deep drawing and the forming configurations.

Experimental set-ups

- Hemisphere set-up (Fig. 3): a traditional set-up to calibrate models and validate them. No blank holder is used in this set-up, only loading is considered and both models are evaluated.

The hemisphere set-up was only composed of one hemispherical punch. The simulation followed the same guidelines as presented in the forming process section. The results are given in Fig. 7 and Fig. 8 and discussed in the next section.

- Four-branch cross set-up (Fig. 4): this experiment implies the use of a cross as a mold and four independent punches. It was first used to compare the hyperelasticity and hysteretic approaches for complex deep drawing. The next section shows the limits of the hyperelastic model when using this set-up. It is also employed in the last part of the paper in the context of new draping strategies such as incremental forming. No blank holder is used in this set-up, loading and unloading are both considered (with different sequences presented in Table. 8 and both models are evaluated).
- T-shape set-up (Fig. 5): this is an alternative version of the four-branch cross composed of three punches and three blank holders. This set-up was used in the last part and the results gave rise to a discussion about incremental forming possibilities. Blank holders were used in this set-up. They followed a prescribed displacement (at a constant speed of $1mm.s^{-1}$) until they slightly touch the fabric without applying any pressure. Only loading is considered (with different sequences presented in Table. 8. Only the hysteretic approach is used).

Material and lay-up configuration

A 2.5D interlock woven fabric made of continuous carbon fibers was used for each experiment. The main fabric properties are listed in Table 1.

Based on Wendling et al. [55, 56], the friction coefficient between the fabric and the mold could be determined and was set to 0.2. The dimensions of a single ply were 400 x 400 mm.

Three configurations, listed in Table. 2, were tested. However, interesting results are mainly obtained from the C_2 configuration wherefore only this configuration is presented in this paper.

Finite element, calculation software and procedure

Each simulation was carried out by using a rotation-free element of type S3 requiring three neighbors to define the out-of-plane bending curvature (denoted by χ or C). Initially developed by Sabourin et al. [57], it has been upgraded by Hamila et al. [52]. The curvature is the input parameter for the out-of-plane bending behavior. Concerning the in-plane shear behavior, the product between the contravariant basis in the initial

deformation state and the covariant basis in the deformed state leads to the transformation gradient (noted \mathbf{F}) [58]. This gradient is the input of the in-plane shear model.

The out-of-plane bending model transforms the curvature (warp and weft) into the bending moment (warp and weft) while the in-plane shear model transforms the shear angle calculated from the transformation gradient into the in-plane shear stress.

Parameters identified for each model

As mentioned previously, the tensile stiffness in the warp and weft direction were considered elastic. Consequently, the parameters were the same for both a hyperelastic or hysteretic approach and set to $K_{T1} = K_{T2} = 34500MPa$. Concerning the in-plane shear (described by the components S_{12} and S_{21} of the stress tensor, computed by the shear angle γ) and the out-of-plane bending (described by the momentum M_{11} and M_{22} , computed by the curvature χ_{11} in the warp direction and χ_{22} in the weft), the parameters may be different depending on the hyperelastic or hysteretic approach. First, concerning the in-plane shear, Table 3 gives the parameters identified for the hyperelastic model described by the following equation: $S_{12} = S_{21} = sign(\gamma) \cdot \sum_{i=1}^6 K_i^{sh} \cdot |\gamma|^i$. Concerning the hysteretic model, details can be found in [31, 32]. Parameters for model 3 presented in [31] are listed in Table 4.

As before, the hyperelastic model for the out-of-plan bending is described by the following: $M_{11} = sign(\chi_{11}) \cdot \sum_{i=1}^6 M_i^b \cdot |\chi_{11}|^i$ for the warp direction and $M_{22} = sign(\chi_{22}) \cdot \sum_{i=1}^6 M_i^b \cdot |\chi_{22}|^i$ for the weft direction. The parameters M_i^b are listed in Table 5. Concerning the hysteretic model, details can be found in [31, 32]. Parameters are also listed in Table 6 and the identification procedures are given in [31].

2.3. Relevance of the hysteretic model

This section shows that hysteretic models are not always necessary mainly depending on the kind of load applied to the material under forming. Some geometries will naturally lead to cyclic variations of load in terms of shear or bending. It also provides simulation results from two set-ups (the hemisphere and the four-branch cross). A deeper analysis has been made concerning the four-branch cross since notable differences can be seen by comparing the hyperelastic and the hysteretic approach.

Forming process

For all cases (for the three set-ups, for all sequences and for the configuration C2 from Table. 2), the punch performed a vertical displacement at a constant rate of $1mm.s^{-1}$ with a maximum displacement of $80mm$.

Numerical simulation

The first part of this section describes the ability of the hysteretic model to predict simple cases such as a hemisphere. First, the macroscopic results of both hysteretic (Fig. 7(a)) and hyperelastic (Fig. 7(b)) approaches were compared.

For the sake of simplicity, the two models were compared by using a Kiviat Diagram (each axis represents a quantified characteristic). This led to a detailed analysis of the simulation strategies. In this way, it is possible to easily compare eight data: the minimum/maximum shear angle, the minimum/maximum of the bending curvature on the first graph and the minimum/maximum of the shear stress, the minimum/maximum of the bending moment on a second graph. Fig. 8 shows these results for the hemisphere simulation presented above [and before the punch being removed](#). It can clearly be concluded that for simple loading such as this one, the hystereticity and hyperelasticity approaches led to almost identical results.

Indeed, in terms of shear angle, curvature, stress or even bending moment, the results were very similar. The small differences can be explained by a few points. For example, it can be seen in Fig. 1 and Fig. 2, that the hysteretic behavior was very sensitive to the applied load. Thus, a small variation of load led to a significant variation in stress. Moreover, the hysteretic model can cause some parasitic numerical errors. Damping or mass scaling can help reduce this effect but it definitively represents one of the disadvantages of the model.

The next step in analyzing the hysteretic approach is to apply it to complex geometries and loads. To this end, the four-branch cross was proposed. Moreover a mold was created in order to compare the simulation with an experimental approach of the forming. Fig. 9 shows the different parts of this set-up.

Fig. 9(a) and (b) illustrate simulation results of the hysteretic and the hyperelastic model, respectively. Fig. 9(c) and (d) show a partial cross section of the result of the hysteretic model and of the experiment, respectively while the punches are removed.

Differences between the hysteretic and hyperelastic approaches for this forming are worth further discussion. **The macroscopic shape of the fabric once draped:** In Fig. 9(b), sizable folds appeared on each branch when using the hyperelastic model. These folds were not observed in the experiment. On the contrary, the macroscopic shape resulting from the hysteretic model was much more reliable and closer to reality. This difference can be explained by several points. The most likely cause comes from the analysis of the required deformation energies to deform the fabric. In the case of the unloading, the stresses simulated by the hyperelastic approach can be overestimated. In some cases, it is observable that the energy required to bend the fabric is lower than the energy required to unshear it. Thus, the bending will be overestimated and additional folds will appear. The stresses simulated by the hysteretic approach represent better the experimental observations and do not overestimate as much the energies involved and thus the fabric will perform in another manner. **Fold size and position:** The locations of the folds are not random. They appear exactly where the shear angle is very high, thus resulting in huge variations of load. This observation corresponds well with the previous proposal. **Shear angle mapping:** The shear angle mapping is not the

same in the two approaches. Indeed, since a huge fold was created in Fig. 9(b), it was not possible to bend further, wherefore the in-plane shear mode was activated and created very large unrealistic shear angles. In contrast, the shear field predicted by the hysteretic model (Fig. 9(a)) was more homogeneous and the ratio between bending and shear was better. **Curvature field:** As mentioned before, the curvature field predicted by both models were completely different.

Fig. 10 compares the two approaches using Kiviat diagrams. As demonstrated before the hystereticity model was more realistic than the hyperelasticity approach. This confirms the details given above, although a brief discussion concerning the curvature and bending moment is required. It is important to highlight that for each case, only maximal or minimal values of the shear angle or the curvature (and their associated shear stress or momentum) is proposed. It corresponds to the maximal or minimal values reached during the entire process cycle (loading and unloading). Moreover, since incremental forming is performed, the behavior of the fabric is more complex. The evolution of the shear angle are not necessarily the same for positive or negative angles. For a more standard forming, the evolution is symmetrical, which is not the case for incremental forming. Indeed, the fabric undergoes variations of shear angle going from positive to negative and vice-versa. Regarding the exponential response of the behavior (Fig. 1, a slight variation of angle generates a significant change of stress. Thus, the deformation might be close, but the stress can be more impacted and then turns asymmetrical (as seen Fig. 10. It is also relevant to notice that since bending behavior follows a logarithmic path, even if the maximum curvature value is higher for the F's than for the I's strategy in Fig. 18, the associated momentum remains close. Fig. 11 illustrates the temporal evolution of the shear angle for the four-branch cross set-up. The diagrams result from a post-treatment of the predictions by the hysteretic model. In this context, the following should be mentioned. Firstly, it is clearly visible that the shear angle computed for each finite element gave rise to a huge variation of the load. Indeed, few elements can handle a variation of approximately 40° , which led to a very high variation of stress. Moreover, few elements can also be subject to variations from negative to positive shear angles. Considering the behavior exposed Fig. 1(b), these strong load variations may create important differences in the simulation, as can be seen Fig.14. Secondly, at the simulation time of 200s one can see a small reduction of the shear angle. The same evolution occurred for the out-of-plane bending behavior. This was the so-called springback appeared at the moment at which the punches were removed and the fabric released all the stored energy.

2.4. Hystereticity: benefits and limits

The aim of this subsection is to summarize the benefits and the limits of each model (hyperelastic and hysteretic). Before that, some details and further discussions are given concerning the stored energy and springback effect.

Fig. 12 shows the simulation of a well-known experiment: the Bias-Extension Test. A temporal evolution of the energy is presented in the figure, and as it can be seen the shear angle increased during the specimen loading. Once the desired state was reached, the specimen was released from its clamps and two possibilities emerged. The release of the stored energy in the hyperelastic model (denoted by the letter H in Fig. 12) under unloading occurred very quickly and some numerical effects due to the dynamics of the solver may appear causing the observable vibrations at $t = 42s$. When using the hysteretic model (denoted by the letter D in Fig. 12), only a small amount of energy is generally stored. This led to an improved stability and a strong dynamics phenomena. From the diagram in Fig. 12, it was also possible to numerically quantify the dissipated energy and the spring-back performed by the specimen.

In the case of the cross set-up, only the in-plane shear behavior is numerically analyzed. Both hyperelastic and hysteretic numerical results are presented in Fig. 13. As for the Bias-Extension Test, on the right side of Fig. 13 (hysteretic modeling), there is the residual shear stress field which is different to zero. On the contrary, on the left side of Fig. 13 (hyperelastic modeling), the residual shear stress is getting back to zero. Fig. 14 shows profile of the deformed fabric corresponding to cross-sections marked by a red line in Fig. 13(a) and (d). As can be seen, the spring-back of the fabric was significant and had to be quantified to get further information about the process parameters for the shape optimization of the mold or for the initial geometry of the woven fabric. From a physical point of view, depending on the used model, one deformation mode might dominate the other. As can be seen Fig. 1(b), during unloading, the dissipative approach leads to a sudden drop of the shear stress. However, while using a hyperelastic model, the shear stress remains very high, even above bending stress. It is then overestimated. In that situation, the fabric will rather bend instead of shearing. As a result, much larger folds will appear. This is shown in Fig. 14. On the contrary, when using a dissipative model, the shear energy collapses during unloading, hence the fabric will more likely shear. As a result, bending and then folds decrease.

Moreover, Fig. 14(b) demonstrated that the profiles were very close to each other. Such a small difference between experimental and the numerical approaches may be due to the gravity as it was not considered during the simulation. However, while the punches were in place, the role of the gravity was negligible since the fabric was under pressure or tension. When the punches were removed, gravity was the only remaining load and could therefore deform the fabric.

Table 7 summarizes the advantages and disadvantages of the two models compared in this paper. Based on this comparison it was possible to present some results and give conclusions concerning the incremental forming. This is the aim of the next section.

3. Incremental forming: applications and limits

When it comes to forming parts with a complex geometry, it is common to cut the reinforcement in order to be able to deform the fabric without tearing apart the fibers. Moreover, in some cases, it is also useful to move the preform from one mold to another one. These industrial applications, aiming to release the fabric's stress after draping, may need cyclic load variations (in shear or bending) or may lead to preform cuts that lower the structural properties of the part. Lately, new process strategies have emerged improving the forming capability without damaging the parts. One of them is the incremental forming. To present some novelties when it comes to incremental forming, two set-ups were used: the four-cross branch and the T-shape. The associated sequences are presented in Table 8. It is important to notice that the hysteretical model was applied for each simulation presented here.

3.1. Deep-drawing sequence

Four sequences are made for the four-branch cross and two with the T-shape set-up from Table 8. The approaches were compared with a Kiviat diagram. First, four sequences made for the four-branch cross set-up are considered. (*U, P, F, D* respectively means Unit: one punch at the time; parallel: Punches 1 and 2 first and then punches 3 and 4; Full: All punches at the same time; Diagonal: Punches 1 and 3 first and then punches 2 and 4.) Afterwards, the same work is done for the T-shape preform with the only two sequences (*F* for usual forming and *I* for the incremental forming).

3.2. Forming process

In each case, the punch performed a vertical displacement at a constant rate of $1\text{mm}\cdot\text{s}^{-1}$ with a maximum displacement of 80mm .

3.3. Numerical simulations

The four sequences of the four-branch cross set-up were simulated and compared as follows: First by comparing the macroscopic shape of the fabric (Fig. 15) once draped, and then by comparing the quantitative data (Fig. 16).

In Fig. 15 two mutually orthogonal planes cutting the set-up are illustrated. Several observations were made: The macroscopic shape of the draped fabric is directly linked to the chosen deep-drawing sequence (see section. 3.1). The forming quality was thus sequence-dependent. Moreover, the incremental approach can lead to an inferior result as opposed to regular approach. For example, the *P* strategy gave a worse geometry in terms of wrinkles than the *F* method. Nevertheless, the *D* strategy drastically reduced the value of the curvature, making the wrinkles and folds smoother. Since the shear angle and the curvatures may be reduced depending on the sequence, the residual stress and strains were lower. The spring-back effect would be handled in a better way if the stress inside the material was reduced. As an example, the

P sequence introduced a very huge shear stress, causing a high spring-back and a significant geometrical distortion of the fabric. In a case when the resin is injected just after the forming of the fabric, the internal stresses will be large. This can have an impact on the characteristics of the final part and lead to geometrical distortions.

To conclude, we can state that incremental forming can give a better macroscopic shape while reducing material flaws (lower folds, better shear angles and curvature, less spring-back). However, one of the biggest problems of this method is the process time. The fact of using different punches increases the transformation time of the fabric. This point cannot be neglected from an industrial point of view. But as a first approach, it can be a good option to improve the capacity and the ability of the Resin Transfert Molding process so as to create complex composite parts.

The remaining part of this section concerns the T-shape process. It was shown that even if the final macroscopic shape was improved (Fig. 17), the intrinsic data of the fabric (shear angle, curvature) deteriorated (Fig. 18). This means that, as it is often the case, a compromise is required.

It was clearly visible that the incremental approach gave a much better result in terms of the shape than the regular forming. Indeed, a very huge fold appeared and the fabric did not fit the mold when using the conventional approach. The incremental one led to better draping with just two small folds which were easy to handle with a blank-holder for example.

To conclude, it is shown Fig. 16 and in Fig. 18 that an improvement of the macroscopic geometry by reducing the folds is counterbalanced by an increase of the shear angle. It can also be noted that in some situations, a badly chosen incremental sequence may ruin the reinforcement or enlarge the wrinkles. Fig. 16 and Fig. 18 illustrate these phenomena. Fig. 16 shows that the parallel forming strategy P is not well adapted since it generates larger curvatures than usual forming strategies. Fig. 18 also illustrates the need to compromise by choosing a specific optimization criterion. If the aim is to reduce in plane shearing, then a common forming strategy should be used. On the other hand, if the aim is to reduce the folds and the level of curvature, it would be more efficient to adopt the incremental one.

4. Conclusion

This paper has two different ways to predict the mechanical behavior of composite reinforcements during forming. A comparison between the usual hyperelastic approaches and the new hysteretical ones was first presented. In a second step, a discussion on the advantages and disadvantages of each approach (elastic and hysteretic) made it possible to elaborate an objective opinion, in coherence with the requirements of the simulations. It has been shown that the use of a sophisticated hysteretic model is not mandatory and depends on the complexity of the shape and of the load. If the geometry and the draping process are not

complicated and do not induce a cyclic variation of load, then common models, which are simpler, faster and easily integrable into a calculation software can be applied. However, in order to get the geometrical distortions induced by the transformation process, to determine the elastic spring-back or even the energy dissipated by the shaping, the hysteretic approach is more suitable.

The second part of this paper discussed incremental forming from the point of view of macroscopical geometry and reduction of wrinkling/folds. Here, compromises are necessary, and although the geometry was improved by this process, characteristics such as shear angles, curvature or tension in the fibers can be high. This can affect the material health of the finished part. This is a first study on incremental forming, and caution must be taken. However, future work will go beyond the analysis of the in-situ material health after being formed following incremental strategy. Nevertheless, this approach opens new possibilities for draping complex geometries, as this often requires the fabric to be cut into different parts.

Further works should be made with further in-situ analysis during the forming process from an experimental point of view. Moreover, in terms of simulation, a coupling with the second phase of the RTM process may be interesting. Indeed, considering the statement of the reinforcement as an input parameter for the resin injection phase could give relevant information. Also, some works on thermoforming considering dissipative models coupled with viscoelasticity or viscoplasticity may offer a wide range of perspectives to handle residual stresses or geometrical distortions.

5. Appendix A

In this appendix, a brief description of the models are presented. First for the in-plane shear model, as it a dissipative approach, it is necessary to describe a yield function and the behavioral law which link the stress to the deformation.

$$\begin{cases} f_s(\gamma_p) &= \left| \mu K_{sh} (F_{11}F_{21} + F_{12}F_{22} - \sin(\gamma_p)) - \sum_{i=1}^4 Q_i \gamma_p^i \right| - \left(S_y + \sum_{i=1}^4 A_i \gamma_p^i \right) \\ E_{e12} &= \frac{1}{2} \cdot (F_{11}F_{12} + F_{21}F_{22} - \sin\frac{\gamma_p}{2}) \\ S_{12} &= \mu K_{sh} E_{e12} \end{cases} \quad (1)$$

Where f_s is the yield function, γ_p is the dissipative part of the shear angle, F_{ij} are the component of the transformation gradient under large strains \mathbf{F} and all other value are given in Table 4.

Eq. 1 is the general description. However, for each part (corresponding to $P1$, $P2$, $P3$ and $P4$ in Fig. X) the is an associated formalism:

$$S_{12} = \begin{cases} K_{sh} E_{e12} & \text{if } P_1 \\ K_{sh} E_{e12} & \text{if } P_2 \\ \frac{1}{2} S_0 + \mu \cdot K_{sh} \cdot \left[\sum_{m=0}^3 B_m^{sh} |S_0|^m \right] \cdot \text{sign}(\gamma - \gamma_0) \cdot \frac{\Gamma(2)}{\Gamma(2-\alpha)} \cdot |\gamma - \gamma_0|^{1-\alpha} & \text{if } P_3 \\ K_{sh} E_{e12} & \text{if } P_4 \end{cases} \quad (2)$$

Where S_0 and γ_0 are respectively the value of the shear stress and the value of the shear angle when the loop (phase $P3$) starts. As an exemple, in Fig. 1, for the second loop, $S_0 = 0.66$ and $\gamma_0 = 21$. Briefly, it represent the hystory of the material.

To model the bending behavior, the idea is the same by using the fractional derivative theory for $P2$ and $P3$:

$$M_{11} = M_{22} = \begin{cases} M_{max} \cdot (1 - \exp(-\frac{\chi}{K})) & \text{if } P_1 \\ M_0 + \left[\sum_{b=0}^8 B_b |\chi|^b \right] \cdot \text{sign}(\chi - \chi_0) \cdot \frac{\Gamma(2)}{\Gamma(2-\beta)} \cdot |\chi - \chi_0|^{1-\beta} & \text{if } P_2 \\ M_1 + \left[\sum_{b=0}^8 B_b |\chi|^b \right] \cdot \text{sign}(\chi - \chi_1) \cdot \frac{\Gamma(2)}{\Gamma(2-\beta)} \cdot |\chi - \chi_1|^{1-\beta} & \text{if } P_3 \end{cases} \quad (3)$$

Where M_{max} is the upper limit on the momentum, χ is the value of the curvature, χ_0 , M_0 are respectively the value of the curvature and momentum when the phase P2 starts (hysteresis loop descent), χ_1 , M_1 are respectively the value of the curvature and momentum when the phase P3 starts (hysteresis loop ascent) and the other value are given in Table 6.

As previously specified, 11 variables have to be identified: seven in-plane variables (μ , K_{sh} , A_i , Q_i , S_y , the derivative order (α) and the fractional derivative coefficient (B_{sh}) and four out-of-plane bending (K , M_{max} , β and B_b). μ is assumed equal to 1 and the parameters A_i , B_i and K_{sh} consider this assumption. K_{sh} is the stiffness corresponding to the linear evolution at the load beginning. It is directly collected from the experimental in-plane shear curve. S_y is the elastic limit which is also picked from the experimental curve. It corresponds to the end of the linear behavior. A_i and B_i related to the isotropic and kinematic hardening functions and are identified by fitting the experimental result. α and B_{sh} are identified from an inverse approach to fit the model with the experiment. Moreover, B_{sh} is supposed to be a function of S_0 through a polynomial function (of order 3). Concerning the bending model, M_{max} and K are directly collected from the experimental curve (Fig. 2). The fractional derivatives parameters are then identified through an inverse approach to fit the model.

Since the fractional derivatives is a very sensitive numerical tool, high digit precision is needed to properly describe the behavior.

References

- [1] E. De Bilbao, D. Soulat, G. Hivet, A. Gasser, Experimental study of bending behaviour of reinforcements, *Experimental Mechanics* 50 (3) (2010) 333–351.
- [2] T. Lahey, Modelling hysteresis in the bending of fabrics, Ph.D. thesis, University of Waterloo (2002).
- [3] W. R. Yu, M. Zampaloni, F. Pourboghraat, K. Chung, T. J. Kang, Analysis of flexible bending behavior of woven preform using non-orthogonal constitutive equation, *Composites Part A: Applied Science and Manufacturing* 36 (6) (2005) 839–850.
- [4] B. Liang, P. Chaudet, P. Boisse, Curvature determination in the bending test of continuous fibre reinforcements, *Strain* 53 (1) (2017) e12213.

- [5] G. H. Philippe Boisse, Jean Launay, Experimental analysis of the influence of tensions on in plane shear behaviour of woven composite reinforcements, ScienceDirect, 2010.
- [6] M. H. Kashani, A. Rashidi, B. Crawford, A. Milani, Analysis of a two-way tension-shear coupling in woven fabrics under combined loading tests: Global to local transformation of non-orthogonal normalized forces and displacements, Composites Part A: Applied Science and Manufacturing 88 (2016) 272–285.
- [7] M. Komeili, A. Milani, On effect of shear-tension coupling in forming simulation of woven fabric reinforcements, Composites Part B: Engineering 99 (2016) 17–29.
- [8] M. H. Kashani, A. Hosseini, F. Sassani, F. Ko, A. Milani, Understanding different types of coupling in mechanical behavior of woven fabric reinforcements: A critical review and analysis, Composite Structures 179 (2017) 558–567.
- [9] K. D. Potter, The early history of the resin transfer moulding process for aerospace applications, Composites Part A : Applied Science and Manufacturing, pp: 619-621, 1999.
- [10] R. Parnas, Liquid composite molding, Garner Publications, 2000.
- [11] A. Jacob, Bmw counts on carbon fibre for its megacity vehicle, Reinforced plastics 54 (5) (2010) 38–41.
- [12] M. Komeili, A. S. Milani, Shear response of woven fabric composites under meso-level uncertainties, Journal of Composite Materials 47 (19) (2013) 2331–2341.
- [13] M. Komeili, Mechanical behavior of woven fabric composites under meso-level uncertainties: modeling and sensitivity analysis, Ph.D. thesis, University of British Columbia (2010).
- [14] M. Komeili, A. Milani, An elaboration on the shear characterization of dry woven fabrics using trellising tests, Polymer Composites 34 (3) (2013) 359–367.
- [15] S. Kawabata, M. Niwa, H. Kawai, Finite-deformation theory of plain-weave fabrics - 3. the shear-deformation theory, Journal of the textile institute 64 (2) (1973) 62–85.
- [16] X. Peng, J. Cao, A continuum mechanics-based non-orthogonal constitutive model for woven composite fabrics, Composites Part A: Applied Science and Manufacturing (2005).
- [17] P. Xue, X. Peng, J. Cao, A non-orthogonal constitutive model for characterizing woven composites, Composites part A: Applied Science and manufacturing 34 (2) (2003) 183–193.
- [18] L. Daelemans, J. Faes, S. Allaoui, G. Hivet, M. Dierick, L. Van Hoorebeke, W. Van Paepegem, Finite element simulation of the woven geometry and mechanical behaviour of a 3d woven dry fabric under tensile and shear loading using the digital element method, Composites Science and Technology 137 (2016) 177–187.
- [19] A. Charmetant, J. G. Orliac, E. Vidal-Sallé, P. Boisse, Hyperelastic model for large deformation analyses of 3d interlock composite preforms, Composites Science and Technology 72 (12) (2012) 1352–1360.
- [20] M. Selezneva, N. Naouar, Y. Denis, L. Gorbatikh, P. Hine, S. V. Lomov, Y. Swolfs, I. Verpoest, P. Boisse, Identification and validation of a hyperelastic model for self-reinforced polypropylene draping, International Journal of Material Forming (2020) 1–11.
- [21] T. Gereke, O. Döbrich, M. Hübner, C. Cherif, [Experimental and computational composite textile reinforcement forming: A review](#), Composites Part A: Applied Science and Manufacturing 46 (2013) 1–10. doi:<https://doi.org/10.1016/j.compositesa.2012.10.004>.
URL <https://www.sciencedirect.com/science/article/pii/S1359835X12003211>
- [22] M. F. Aliabadi, Woven composites, Vol. 6, World Scientific, 2015.
- [23] L. Montero, S. Allaoui, G. Hivet, Characterisation of the mesoscopic and macroscopic friction behaviours of glass plain weave reinforcement, Composites Part A: Applied Science and Manufacturing 95 (2017) 257–266.
- [24] S. Allaoui, G. Hivet, A. Wendling, D. Soulat, S. Chatel, [Experimental approach for optimizing dry fabric formability](#), in: 14th European Conference on Composite Materials, Budapest, Hungary, 2010, pp. ID347–ECCM14.
URL <https://hal.archives-ouvertes.fr/hal-00634677>

- [25] E. Guzman-Maldonado, N. Hamila, N. Naouar, G. Moulin, P. Boisse, Simulation of thermoplastic prepreg thermoforming based on a visco-hyperelastic model and a thermal homogenization, *Materials & Design* 93 (2016) 431–442.
- [26] D. Dörr, F. J. Schirmaier, F. Henning, L. Kärger, A viscoelastic approach for modeling bending behavior in finite element forming simulation of continuously fiber reinforced composites, *Composites Part A: Applied Science and Manufacturing* 94 (2017) 113–123.
- [27] D. Dörr, F. Henning, L. Kärger, Nonlinear hyperviscoelastic modelling of intra-ply deformation behaviour in finite element forming simulation of continuously fibre-reinforced thermoplastics, *Composites Part A: Applied Science and Manufacturing* 109 (2018) 585–596.
- [28] J. C. Simo, A framework for finite strain elastoplasticity based on maximum plastic dissipation and the multiplicative decomposition: Part i. continuum formulation, *Computer methods in applied mechanics and engineering* 66 (2) (1988) 199–219.
- [29] J.-L. Chaboche, Time independent constitutive theories for cyclic plasticity, *International Journal of Plasticity* PP: 149 - 188, 1986.
- [30] T. A. Ghafour, J. Colmars, P. Boisse, The importance of taking into account behavior irreversibilities when simulating the forming of textile composite reinforcements, *Composites Part A: Applied Science and Manufacturing* 127 (2019) 105641.
- [31] Y. Denis, F. Morestin, N. Hamila, A hysteretic model for fiber-reinforced composites at finite strains: fractional derivatives, computational aspects and analysis, *Computational Materials Science* 181 (2020) 109716.
- [32] Y. Denis, E. Guzman-Maldonado, N. Hamila, J. Colmars, F. Morestin, A dissipative constitutive model for woven composite fabric under large strain, *Composites Part A: Applied Science and Manufacturing* 105 (2018) 165–179.
- [33] J. Wojewoda, A. Stefański, M. Wiercigroch, T. Kapitaniak, Hysteretic effects of dry friction: modelling and experimental studies, *Philosophical Transactions of the Royal Society A: Mathematical, Physical and Engineering Sciences* 366 (1866) (2008) 747–765.
- [34] A. Krasnobrizha, P. Rozycki, L. Gornet, P. Cosson, Hysteresis behaviour modelling of woven composite using a collaborative elastoplastic damage model with fractional derivatives, *Composite Structures* 158 (2016) 101–111.
- [35] R. T. Faal, R. Sourki, B. Crawford, R. Vaziri, A. S. Milani, Using fractional derivatives for improved viscoelastic modeling of textile composites. part i: Fabric yarns, *Journal of Composite Materials* (2020) 0021998320912479.
- [36] R. Faal, R. Sourki, B. Crawford, R. Vaziri, A. Milani, Using fractional derivatives for improved viscoelastic modeling of textile composites. part ii: Fabric under different temperatures, *Composite Structures* (2020) 112494.
- [37] L. Liu, J. Chen, X. Li, J. Sherwood, Two-dimensional macro-mechanics shear models of woven fabrics, *Composites Part A: Applied science and manufacturing* 36 (1) (2005) 105–114.
- [38] P. Harrison, M. Clifford, A. Long, Shear characterisation of viscous woven textile composites: a comparison between picture frame and bias extension experiments, *Composites Science and Technology* 64 (10) (2004) 1453–1465.
- [39] B. P. Cao J., Akkerman R., Characterization of mechanical behavior of woven fabrics : Experimental methods and benchmark results, *Composites Part A : Applied Science and Manufacturing*, p. 1037-1053, 2008.
- [40] D. F. Walczyk, J. F. Hosford, J. M. Papazian, Using reconfigurable tooling and surface heating for incremental forming of composite aircraft parts, *J. Manuf. Sci. Eng.* 125 (2) (2003) 333–343.
- [41] K. A. Al-Ghamdi, G. Hussain, On the comparison of formability of roll-bonded steel-cu composite sheet metal in incremental forming and stamping processes, *The International Journal of Advanced Manufacturing Technology* 87 (1-4) (2016) 267–278.
- [42] M. Fiorotto, M. Sorgente, G. Lucchetta, Preliminary studies on single point incremental forming for composite materials, *International Journal of Material Forming* 3 (1) (2010) 951–954.
- [43] S. Coutandin, D. Brandt, P. Heinemann, P. Ruhland, J. Fleischer, Influence of punch sequence and prediction of wrinkling in textile forming with a multi-punch tool, *Production Engineering* 12 (6) (2018) 779–788.

- [44] Y. Dafalias, E. Popov, A model of nonlinearly hardening materials for complex loading, *Acta mechanica* 21 (3) (1975) 173–192.
- [45] P. A. Eisenberg M.A., On Nonlinear Kinematic Hardening, *Acta Mech*, 1968.
- [46] Z. MRoz, On the description of anisotropic workhardening, *Journal of Mechanic, Physics. Solids*, 1967.
- [47] H. Ziegler, *The Theory of Plasticity : A Survey of Recent Achievements*, James Clayton Lecture, 1955.
- [48] H. Ziegler, A modification of Prager’s hardening rule, *Brown University*, pp: 55-65, 1959.
- [49] G. Lebrun, M. N. Bureau, J. Denault, Evaluation of bias-extension and picture-frame test methods for the measurement of intraply shear properties of pp/glass commingled fabrics, *Composite structures* 61 (4) (2003) 341–352.
- [50] X. Peng, J. Cao, J. Chen, P. Xue, D. Lussier, L. Liu, Experimental and numerical analysis on normalization of picture frame tests for composite materials, *Composites Science and Technology* 64 (1) (2004) 11–21.
- [51] S. V. Lomov, A. Willems, I. Verpoest, Y. Zhu, M. Barburski, T. Stoilova, Picture frame test of woven composite reinforcements with a full-field strain registration, *Textile Research Journal* 76 (3) (2006) 243–252.
- [52] N. Hamila, P. Boisse, F. Sabourin, M. Brunet, A semi-discrete shell finite element for textile composite reinforcement forming simulation, *International journal for numerical methods in engineering* 79 (12) (2009) 1443–1466.
- [53] T. Kawabata, Y. Takezono, T. Kanai, O. Izumi, Bend tests and fracture mechanism of tial single crystals at 293–1073 k, *Acta Metallurgica* 36 (4) (1988) 963–975.
- [54] J. Huang, P. Boisse, N. Hamila, Y. Zhu, Simulation of wrinkling during bending of composite reinforcement laminates, *Materials* 13 (10) (2020) 2374.
- [55] A. Wendling, G. Hivet, E. Vidal-Sallé, P. Boisse, Consistent geometrical modelling of interlock fabrics, *Finite Elements in Analysis and Design* 90 (2014) 93–105.
- [56] G. Hivet, S. Allaoui, D. Soulat, A. Wendling, S. Chatel, Analysis of woven reinforcement preforming using an experimental approach, *arXiv preprint arXiv:1110.5178* (2011).
- [57] F. Sabourin, M. Brunet, Detailed formulation of the rotation-free triangular element “s3” for general purpose shell analysis, *Engineering computations* (2006).
- [58] T. Belytschko, W. K. Liu, B. Moran, K. Elkhodary, *Nonlinear finite elements for continua and structures*, John wiley & sons, 2013.

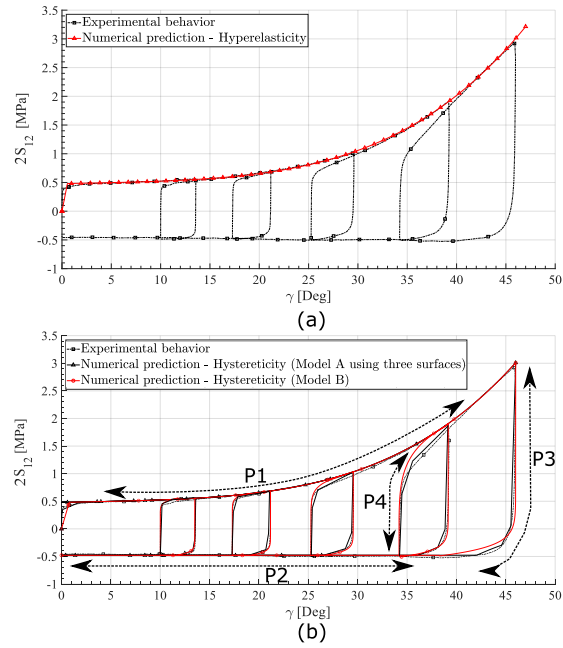


Figure 1: Comparison between experimental results and hyperelasticity (a) or hysteresicity (b) constitutive laws for the in-plane shear deformation mode.

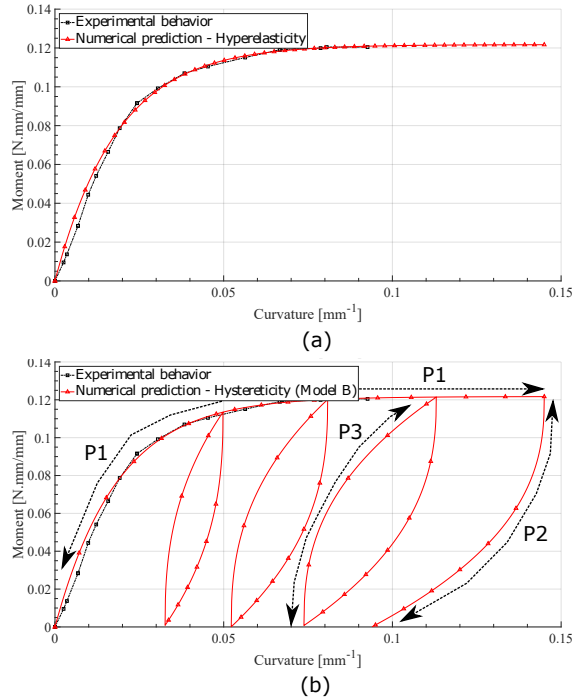


Figure 2: Comparison between experimental results and hyperelasticity (a) or hysteresicity (b) constitutive laws for the out-of-plane bending deformation mode.

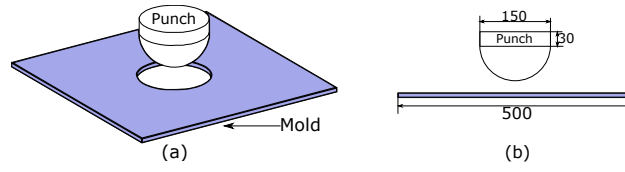


Figure 3: Experimental set-up for a hemisphere: configuration and dimensions (in mm).

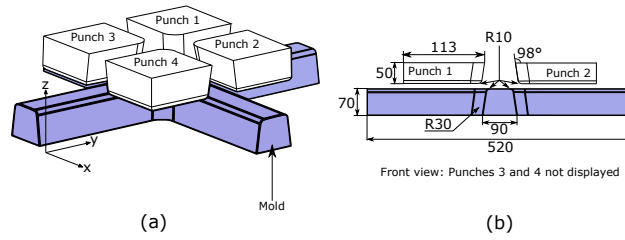


Figure 4: Experimental set-up for a four-branch cross: configuration and dimensions (in mm).

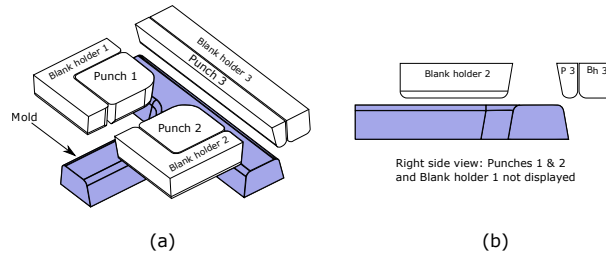


Figure 5: Experimental set-up for a T-shape: configuration and dimensions (in mm). (BH: Blank-holder, P: Punch).

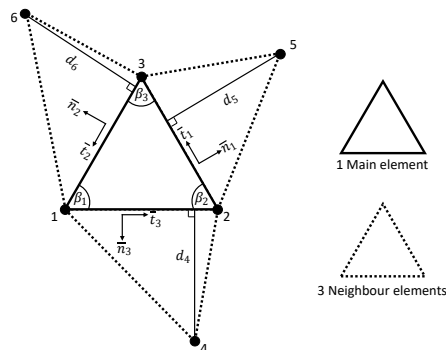


Figure 6: Rotation-free S3 element and its three neighbors [52].

Material Properties

Reference	Hexcel®G1151
Area density (g/m ²)	630
Weave style	2.5D Interlock 3X/Formable
Distribution (%) (Warp / Weft)	51 / 49
Warp density (Yarns/cm)	7.4
Weft density (Yarns/cm)	7.4
Type of yarn	T300JB 6K 40D HR
Standard length (mm)	1000
Thickness (mm)	0.62
Powdered	Yes (2.5% per side)
Yarn material	Carbone

Table 1: Main **Hexcel®G1151** fabric properties.

Configuration	Nb of plies	Lay-up
C_1	1	$[0^\circ/90^\circ]_1$
C_2	1	$[-45^\circ/45^\circ]_1$
C_3	1	$[-30^\circ/60^\circ]_1$

Table 2: Lay-up configurations.

Shear mode, identified parameters for hyperelasticity

Parameters	Value
K_1^{sh}	0.0068985606590104
K_2^{sh}	-1.373399e-04
K_3^{sh}	9.334663e-06
K_4^{sh}	-5.6856887e-07
K_5^{sh}	1.194473e-08
K_6^{sh}	-6.776111e-11

Table 3: Main **Hexcel®G1151** in-plane shear properties for the hyperelastic model.

Shear mode, identified parameters for hystereticity	
Parameters	Value
K_{sh}	10
$A_1 Q_1$	-6.51941e-04
$A_2 Q_2$	3.39666e-04
$A_3 Q_3$	-1.52940e-05
$A_4 Q_4$	2.27941e-07
$A_5 Q_5$	-6.42145e-10
S_y	0.0311
μ	1
α	0.93
B_{sh}^0	0.00248731
B_{sh}^1	0.06172057
B_{sh}^2	-0.0172634
B_{sh}^3	0.01018563

Table 4: Main **Hexcel®G1151** in-plane shear properties for the hysteretic model.

Bending mode, identified parameters for hyperelasticity	
Parameters	Value
M_1^b	9.73393
M_2^b	-43.495389
M_3^b	108.713715
M_4^b	-148.130337
M_5^b	103.274319
M_6^b	-28.70461

Table 5: Main **Hexcel®G1151** out-of-plane bending properties for the hyperelastic model.

Bending mode, identified parameters for hystereticity	
Parameters	Value
M_{max}	0.12
K	0.0185
β	0.6
B_b^0	0.67689986
B_b^1	30.9022174
B_b^2	-2.38369655e+02
B_b^3	9.62818548e+02
B_b^4	-2.33408327e+03
B_b^5	3.51477203e+03
B_b^6	-3.22136641e+03
B_b^7	1.64652542e+03
B_b^8	-3.59189579e+02

Table 6: Main **Hexcel®G1151** out-of-plane bending properties for the hysteretic model.

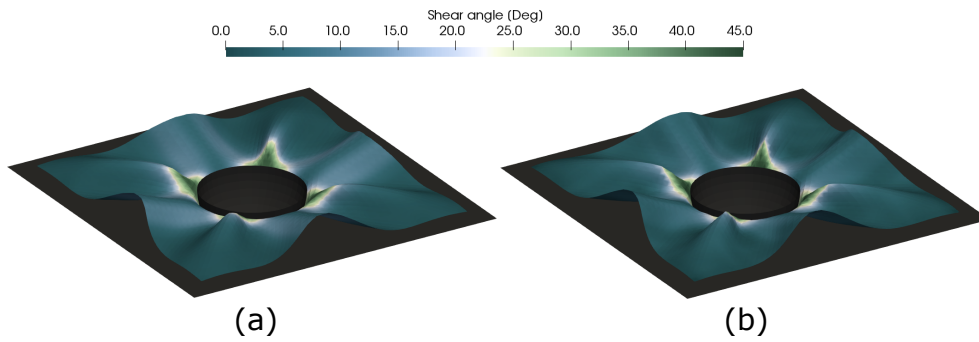


Figure 7: Simulation results of a hemisphere deep-drawing using a hysteretic model (a) and a hyperelastic model (b). Visualization of the macroscopical shape and shear fields. Punch unremoved.

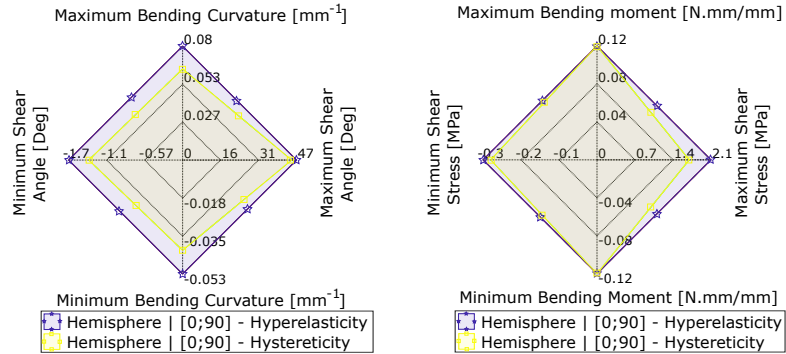


Figure 8: Graphs comparing the hyperelastic and the hysteretic approaches for a simulation of hemisphere deep-drawing. Curvature and shear angle on the left, bending moment and shear stress on the right. Punch unremoved.

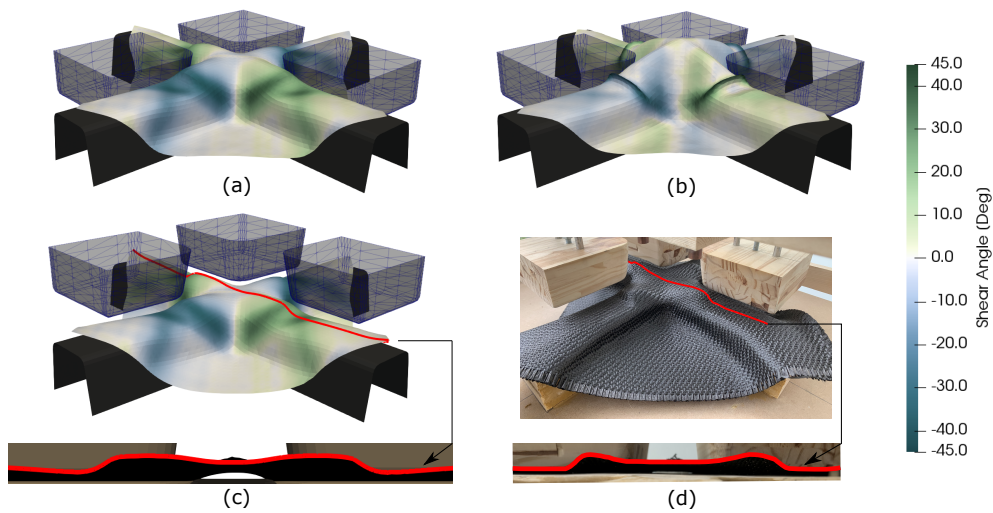


Figure 9: Comparison of the simulation with an experiment involving four-branch cross deep-drawing. The punch nb 4 has been removed for clarity. Results obtained with a hysteretic model before unloading (a), with a hyperelastic model before unloading (b), a cross section through the simulated (hysteretic) fabric after unloading (c) and through the experimental fabric after unloading (d).

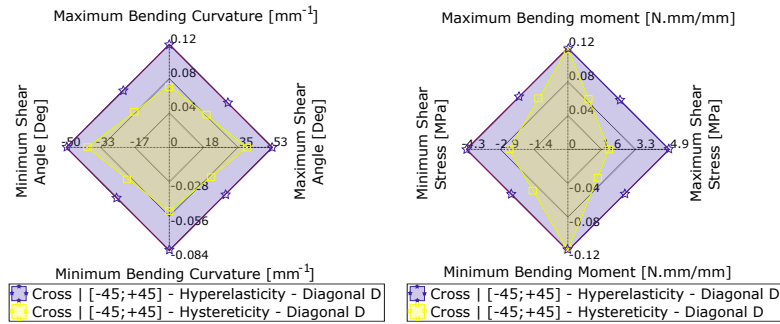


Figure 10: Graphs comparing the hyperelastic and the hysteretic approaches for a four branches cross deep-drawing simulation. Curvature and shear angle on the left, bending moment and shear stress on the right. The imposed load followed the sequence $S_n4 : D$ proposed in Table 8.

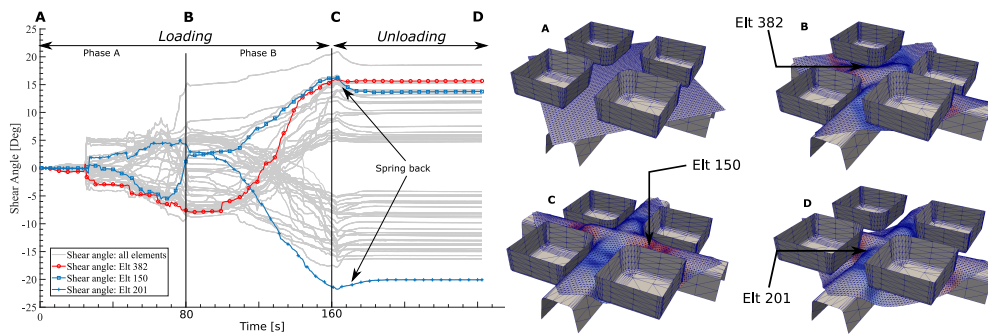


Figure 11: Evolution of the shear angle in a fabric region during a four-branch cross deep-drawing simulation. The imposed load followed the sequence $S_n4 : D$ proposed in Table 8.

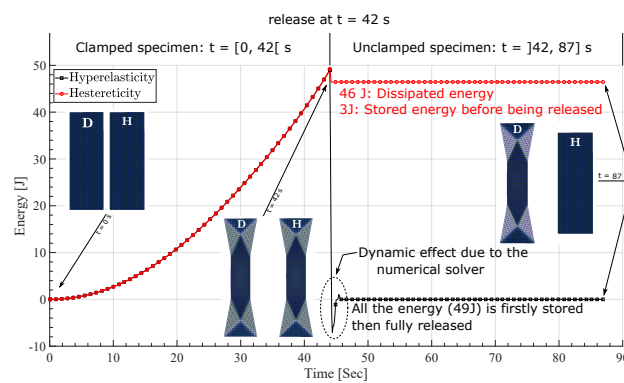


Figure 12: Comparison between hyperelasticity and hystereticity for the in-plane shear deformation mode (on Hexcel GG1151 reinforcement). Abbreviations D and H respectively means Dissipative (or Hysteretic) and Hyperleastic approaches.

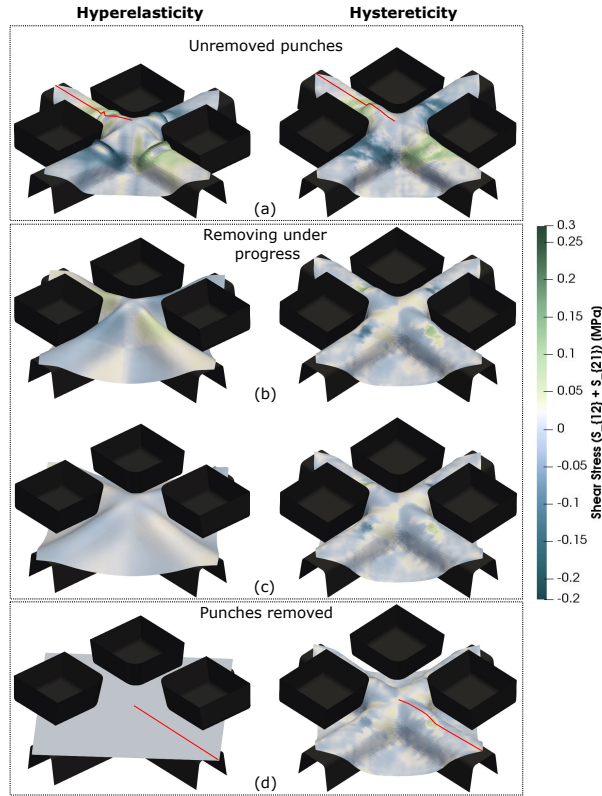


Figure 13: Comparison between hyperelasticity and hysteresis for a cross shape simulation. Punches are not removed (a), final statement of the deformation; punches are removed (b and c), evolution of the spring-back; final statement of the fabric once the punches are removed (d). All the four punches moved at the same time (imposed load F from Table. 8)

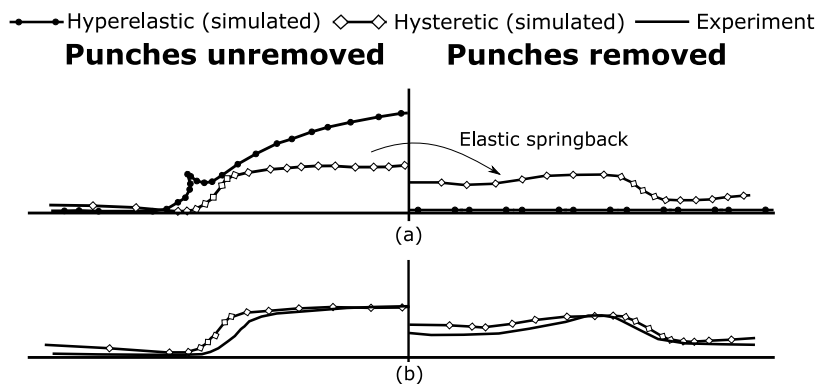


Figure 14: Comparison between fabric profile using hyperelasticity and hysteresis (a) and between the simulation and the experiment (b) when the punches were either unremoved or removed.

	Hyperelasticity	Hystereticity
Simple forming simulation ability	Yes	Yes
Complex forming simulation ability	No	Yes
Model complexity	Low	High
Thermodynamically admissible	Yes	No (not yet)
Energy quantification	No	Yes
Elastic Spring-back	No	Yes
Residual stress	No	Yes
Software intergration	Easy	Hard
Numerical sensibility	Low	High
Incremental forming ability	No	Yes

Table 7: Positive and negative aspects of the hyperelasticity and hystereticity approaches.

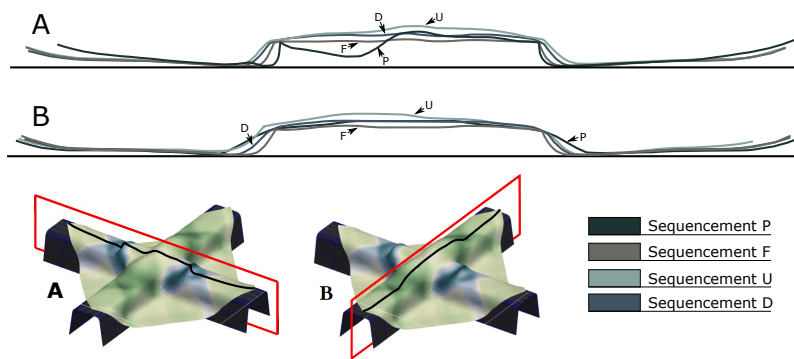


Figure 15: Comparison between different sequences for a four-branch cross set-up and by using hysteretic modeling.

Sequence	Time t [sec]	
Four-branch cross		
Time t [sec]	[0, 80[[80, 160[
S_{n1} :U	P_1	P_2
S_{n2} :P	$P_{1,2}$	$P_{3,4}$
S_{n3} :F	$P_{1,2,3,4}$	-
S_{n4} :D	$P_{2,3}$	$P_{1,4}$
Time t [sec]	[160, 240[[240,320]
S_{n1} :U	P_3	P_4
S_{n2} :P	-	-
S_{n3} :F	-	-
S_{n4} :D	-	-
T shape		
Time t [sec]	[0, 80[[80, 160[
S_{n1} :F	$BH_{1,2,3}, P_{1,2,3}$	-
S_{n2} :I	$BH_{1,2,3}$	$P_{2,3}$
Time t [sec]	[160, 240[[240,320]
S_{n1} :F	-	-
S_{n2} :I	P_1	-

Table 8: Sequences employed for the simulation in Fig. 15 and Fig. 17. (BH: Blank-holder, P: Punch).

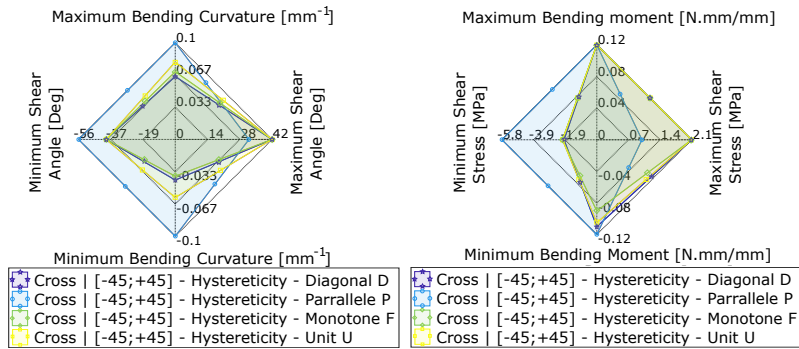


Figure 16: Graphs comparing shear angle/curvatures on the left and shear stress/bending moment on the right for each forming sequences of a four-branch cross.

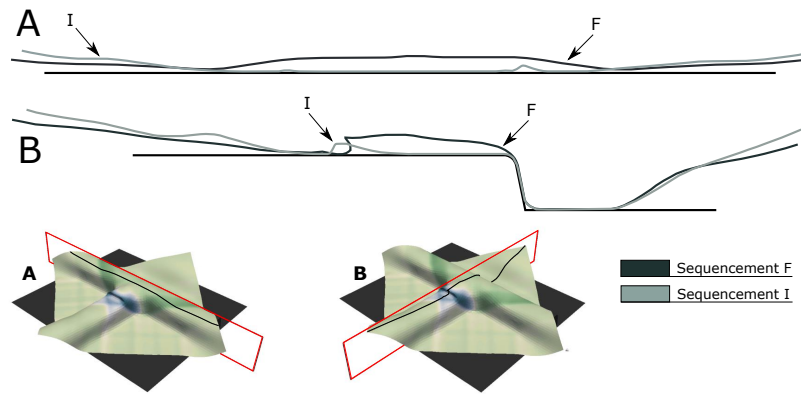


Figure 17: Comparison between hyperelasticity and hysteresis for the in-plane shear deformation mode.

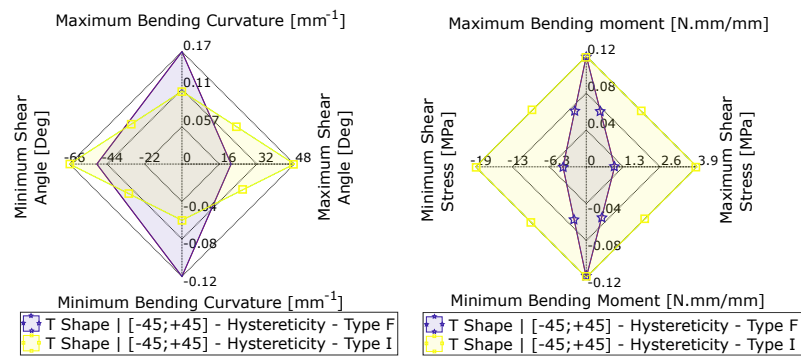


Figure 18: Graphs comparing shear angle/curvatures on the left and shear stress/bending moment on the right for each forming sequences of a T-xshape mold.